Dalton Transactions

PAPER

View Article Online
View Journal | View Issue

Cite this: *Dalton Trans.*, 2018, **47**, 799

A highly stable indium based metal organic framework for efficient arsenic removal from water†

Hala Atallah, [‡a] Mahmoud ELcheikh Mahmoud, [‡a] Feysal M. Ali,[b] Alan Lough[c] and Mohamad Hmadeh [*a]

Received 2nd October 2017, Accepted 4th December 2017

DOI: 10.1039/c7dt03705h

rsc.li/dalton

A new porous indium metal organic framework namely (AUBM-1) was successfully synthesized *via* a solvothermal reaction of pyromellitic acid and indium chloride. Single crystal X-ray analysis revealed the formation of a 3D framework with a **pts** topology. The resulting MOF structure showed high chemical stability at different pH values. Thus, the activated indium MOF was applied for As removal from water for the first time and showed a high arsenate uptake capacity of 103.1 mg g^{-1} at neutral pH, which is higher than the commercial adsorbents (usually less than 100 mg g^{-1} at neutral pH). Finally, the kinetics and thermodynamic studies revealed that the As adsorption was an endothermic process and followed a pseudo-second-order kinetic model.

Introduction

Metal organic frameworks (MOFs) are a new class of materials that are composed of a metal cluster and an organic linker connected to each other *via* coordination bonds and arranged in an extended 3D network.[1,2] Due to their ultrahigh porosity and surface area along with a relatively high thermal and mechanical stability,[3] MOFs are used in numerous applications including catalysis, drug delivery, gas separation, magnetism, conductivity, luminescence and water remediation.[1,2,4–9] One of the most interesting features of MOFs is that every component of their structure can be varied and functionalized to optimize their properties.[10] However, most MOFs are pH sensitive so the synthesis of chemically stable MOFs remains a challenge which limits their applications in aqueous media.[11] Some water stable MOFs such as ZIF-8,[12] MIL-53 [13] and UiO-66 [11] have been developed and applied for water remediation to remove water-soluble and toxic pollutants such as As, which is a global threat due to its toxicity and carcinogenicity. Hence, As has been classified by the World Health Organization (WHO) as the first priority issue among the toxic elements.[11,14] As is found in contaminated ground water usually at concentrations ranging from 0.5 to 3 mg g^{-1}, and in industrial waste water at a much higher concentration (>100 mg g^{-1}) which is much higher than the acceptable range (10 μg l^{-1}).[15,16] Exposure to As-polluted water would cause skin damage, circulatory problems, and an increased risk of cancer.[17] Although aquatic As possesses different oxidation states, inorganic As is usually oxidized to arsenate As(V) in various aqueous media.[18] Due to the high mobility of arsenate species in water streams, considerable attention has been recently paid for the effective removal of aquatic arsenate.[11,18] One of the most simple and inexpensive procedures that operate at ambient temperature for As removal from water is adsorption.[11,15] However, the choice of absorbent is crucial for an efficient adsorption process since the use of conventional adsorbents like activated carbon,[19] activated alumina[20] and powdered zeolite[21] showed low adsorption capacity. Thus, many of the current water-treatment challenges could be resolved or enhanced by the development of new and highly porous adsorbent materials that have a high specific surface area and therefore, the capability to adsorb a large quantity of pollutants.[11,15] Due to their high surface area and customizable chemical functionalities, chemically stable MOFs are good candidates to be used as adsorbents for As removal from wastewater. Although ZIF-8, UiO-66, MIL-53 and Fe-BTC MOF materials have been employed in aquatic As removal, their performance in comparison with other commercial and synthetic adsorbents was not very effective, except for UiO-66 which has recently shown a great capacity for As removal but at low pH (acidic medium). Furthermore, group IIIA metal (Al, In, and Ga) based MOFs (known also as pMOFs) have received considerable attention due to their interesting network topologies,[22] great surface area and high chemical stability.[23] They

[a] Chemistry Department, American University of Beirut, P.O. Box 11-0236, Riad El-Solh, 1107 2020 Beirut, Lebanon. E-mail: mohamad.hmadeh@aub.edu.lb
[b] Department of Materials Science & Engineering, University of Toronto, 184 College Street, Toronto, Ontario, M5S 3E4, Canada
[c] Department of Chemistry, University of Toronto, 80 St George, Toronto, ON M5S 3H6, Canada

† Electronic supplementary information (ESI) available. CCDC 1568434. For ESI and crystallographic data in CIF or other electronic format see DOI: 10.1039/c7dt03705h

‡ These authors contributed equally to this paper.

have been employed in many applications ranging from gas absorption, fluorescence, ion-exchange properties and Lewis acid catalysis.[22] However, these MOF structures represent a minute percentage of the total number of MOF papers reported to date (*ca.* 4%).[24] In this context, developing new pMOF structures and exploring them for new applications remain of particular interest. Herein, we report the synthesis and characterization of a new chemically stable indium-MOF, namely AUBM-1 (AUBM = American University of Beirut Materials) and study its capacity to remove As from water at neutral pH. Besides the novelty of the structure reported, to the best of our knowledge, this is the first study of applying In-MOF in As pollutant removal from water.

Experimental section

Materials and methods

All reagents and solvents employed were commercially available and used without further purification. The infrared (IR) spectra were recorded on a FT-IR spectrometer Thermo-Nicolet working in the transmittance mode, in the 450–3950 cm^{-1} range. Thermogravimetric analysis (TGA) was performed with Netzsch TG 209 F1 Libra apparatus. Powder X-ray diffraction (PXRD) patterns were collected using a Bruker D8 advance X-ray diffractometer (Bruker AXS GmbH, Karlsruhe, Germany) at 40 kV, 40 mA (1600 W) using Cu Kα radiation (k = 1.5418 Å). Scanning electron microscopy (SEM) was performed using a MIRA3 Tescan electron microscope, where the samples were first coated with a thin layer of gold. High-resolution transmission electron microscopy (HRTEM) was performed using a Hitachi HF3300, working at an operation voltage of 300 kV. The Brunauer–Emmett–Teller (BET) surface area was measured using a Quantachrome-NOVA 2200e-Surface Area and Pore Size Analyzer. As concentration was determined using Atomic Absorption Spectroscopy (AAS) conducted with a Thermo Elemental Analyzer.

Synthesis and activation of AUBM-1

In a 20 ml scintillation vial, 2-methylimidazole (105 mg, 1.28 mmol) was dissolved in 15 ml DMF and sonicated for 10 minutes. Following sonication, 1,2,4,5-benzenetetracarboxylic acid (530 mg, 2.1 mmol) was added. After 10 minutes of further sonication, anhydrous $InCl_3$ (185 mg, 0.85 mmol) and 0.4 ml of propionaldehyde were added and the reaction mixture was sonicated for a couple of minutes. The vial was then transferred to an oven set at 150 °C for 5 hours. The resulting white needle-shaped crystals were centrifuged, and the supernatant was discarded. The solids were washed with DMF for 2 d, and the solution was exchanged with fresh DMF three times per day. This was followed by washing with dichloromethane (DCM) for 2 d, and the solution was exchanged with fresh DCM three times per day. The solids were collected by centrifugation and dried under dynamic vacuum at 110 °C for 12 h. The calculated yield was 54%. The AUBM-1 crystals were activated in the furnace at 300 °C for 12 hours, then washed with DCM three times and degassed at 100 °C for 6 h.

Arsenate adsorption experiments

The effect of different experimental conditions on the As removal efficiency was studied by changing several parameters such as pH, temperature, contact time and concentration. For the pH effect experiment, 10 mL arsenate solutions using sodium arsenate dibasic heptahydrate with an initial concentration of 40 mg L^{-1} and 10 mg of activated In-MOF adsorbents were placed in each of six Falcon tubes. These tubes were constantly shaken at the rate of 200 rpm for 12 h at 25 °C. Every tube had a different pH between 2 and 10 which was controlled *via* buffer solutions. For the temperature effect, 10 mL of arsenate solutions (40 mg L^{-1} and pH = 7.6) and 10 mg of activated In-MOF adsorbents were added to each of six Falcon tubes. Each Falcon tube was placed at different temperatures between 25 and 50 °C with 5 °C increment, and they were constantly shaken for 12 h. For the kinetic study, 10 mL arsenate solutions (40 mg L^{-1} and pH = 7.6) and 10 mg of activated In-MOF adsorbents were added to each of ten Falcon tubes, and the tubes were constantly shaken at 25 °C. Each tube was removed at the allocated time from 10 min to 48 h. For the different concentration experiment, 10 mL arsenate solutions of different concentrations ranging from 30 to 200 mg L^{-1} (pH = 7.6) and 10 mg of activated In-MOF adsorbents were mixed in each of nine Falcon tubes and the tubes were constantly shaken for 12 h at 25 °C.

In all the above experiments, the solutions were then filtered through a 0.20 μm filter and the residual As concentrations of the filtrates were measured using atomic absorption spectroscopy.

Arsenic adsorption in the presence of anions

In these experiments, 10 mg of activated In-MOF were added to a 10 ml of 40 ppm As solution in the presence of Na_2CO_3 or $NaNO_3$ in a 15 ml Falcon tube at two different concentrations (1 mM and 10 mM). After a contact time of 12 h at 25 °C under shaking, the solution was filtered and the residual As concentration of the filtrate was measured using atomic absorption spectroscopy.

Arsenic desorption experiment

In a Falcon tube, 10 ml of concentrated NaCl solution (7 M) were added to 10 mg of the As-loaded MOF. The tube was constantly shaken for 12 h. The solution was then filtered through a 0.20 μm filter and the residual As concentration of the filtrate was measured using atomic absorption spectroscopy. This process was repeated three times.

Results and discussion

AUBM-1 crystals were prepared by combining 2.5 equivalents of pyromellitic acid with 1 equivalent of indium chloride in a DMF solution in the presence of 2-methylimidazole and propionaldehyde. The mixture was heated at 150 °C for 5 h to give rice-shaped crystals that are suitable for single crystal X-ray analysis. The crystal structure was solved in the tetragonal space group $P4_2/ncm$. The In atom has $2/m$ site symmetry and is coordinated in a distorted square-antiprismatic coordination geometry by four bridging benzene-1,2,4,5-tetracarboxylate ligands forming a three-dimensional network. The discrete imidazole molecules are disordered over the four-fold inversion axis. The structure of AUBM-1 is composed of an edge transitive net, with two kinds of nodes, a tetrahedral one and a square one of the metal and linker, respectively, to form a 3-D framework of **pts** topology (Fig. 1 and Fig. S1†). This structure is strongly related to a reported In-structure[23] which is also based on a pyromellitic acid linker and indium clusters joined together to form a network with the **pth** topology, which is chiral with hexagonal symmetry. Although this MOF was reported as having the **pts** topology, analysis of its structure shows that it is actually **pth**. **pts** and **pth** are two highly related, different kinds of networks built up from rectangular and tetrahedral nodes. **pts** has a tetragonal symmetry, while **pth** is hexagonal.[25] The In atom, which has +3 oxidation state, coordinates to four benzene-1,2,4,5-tetracarboxylate ligands (charge of −4). This indicates the formation of an anionic framework, which is common in In-MOFs.[24] The methyl-imidazole located within the framework pores is possibly balancing this charge as the imidazolium unit similar to a reported In-MOF where $Et_2NH_2^+$ ions that were located right beneath each In(III) ion compensate for the anionic charges centered around the In(III) ions. Due to the identical C–O bond length, a possibly protonated carboxylate to balance the charges can be excluded. Additionally, these imidazolium units were found in the IR spectrum of the as-synthesized MOF by the characteristic vibrational band of the C=N centered at 1503 and 1507 cm^{-1}.

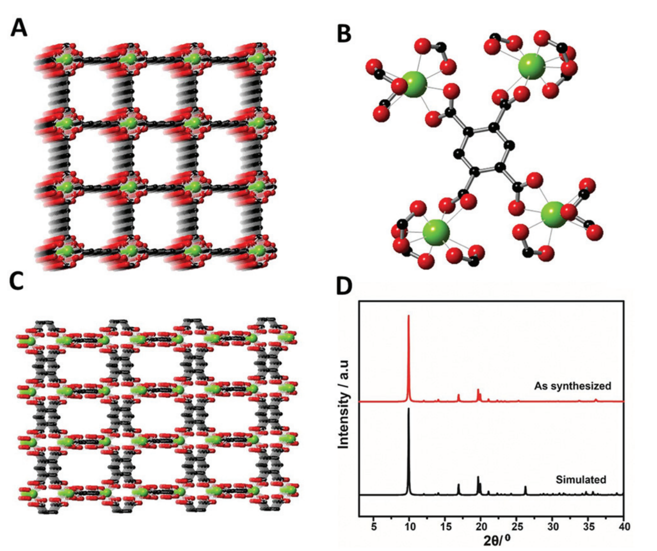

Fig. 1 (A) Crystal structure of AUBM-1 along the *c* axis. Color code: C: black, In: green, O: red, (B) coordination mode of the indium atom by 4 carboxylate units, (C) view along the *b* axis and (D) powder X-ray diffraction (PXRD) pattern of the as-synthesized crystals compared to the simulated one.

The simulated PXRD pattern matches perfectly the experimental one of the as-synthesized sample with no additional peaks, which confirms the high crystallinity and phase purity of the sample (Fig. 1D). The morphology of the crystals was analyzed by HRSEM and HRTEM. The obtained SEM and TEM micrographs of the as-synthesized MOF crystals shown in Fig. 2 revealed the phase purity and homogeneity of the obtained crystals with a uniform rod shape. Fast Fourier transform (FFT) analysis performed on the HRTEM micrographs clearly demonstrates the highly crystalline nature of the as-synthesized structure and confirms the fringe spacing of 0.41 nm and 0.27 nm, which are consistent with the *d*-values of the (110) and (111) reflection planes of the tetragonal AUBM-1, respectively (Fig. 2). It is noteworthy that it is extremely challenging to obtain the HRTEM images of MOF structures due to electron beam damage.[26,27]

In general, it is important that MOFs used for water treatment are chemically stable and do not degrade in aqueous media.[11] Thus, we examined the framework structural stability by soaking it in aqueous solutions at different pH values. PXRD data and SEM images of the samples were collected after the stability test. As shown in Fig. 3A and Fig. S2,† the crystallinity was retained for the tested samples after soaking them in aqueous solutions of pH = 1 to pH = 12 for 3 days. Such a wide range of pH stability has rarely been observed in other reported MOFs.[3,28,29]

The thermal stability of the material was investigated by thermogravimetric analysis (TGA) under a N_2 flow as shown in Fig. 3B. The weight loss profile of the as-synthesized MOF revealed a multipart pattern with several transitions and steps. The initial weight loss at around 150 °C corresponds to the loss of solvent. Then, the unreacted organic species were lost upon increasing the temperature to around 370 °C.[30] Finally, the weight rapidly decreased at about 400 °C indicating the degradation of the framework. The activated sample shows one important weight decrease (*ca.* 40%) at around 430 °C. This demonstrates the good thermal stability of our MOF structure.

To assess the porosity of the MOF structure, the N_2 adsorption/desorption isotherm of the activated sample was obtained, and the Brunauer–Emmett–Teller (BET) surface area was determined to be 310 m^2 g^{-1} (Fig. S3†). This relatively low

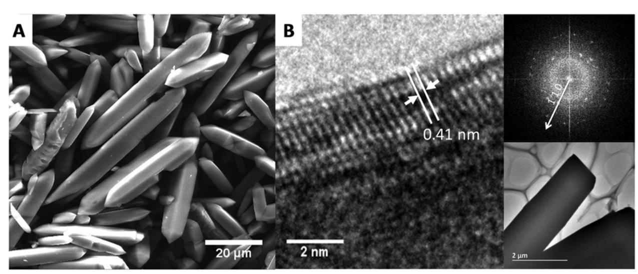

Fig. 2 (A) HRSEM image of AUBM-1 crystals showing uniform morphology and (B) HRTEM image of the AUBM-1 crystals showing the *d*-spacing along with the FFT analysis that shows high crystallinity of the as-synthesized In-MOF.

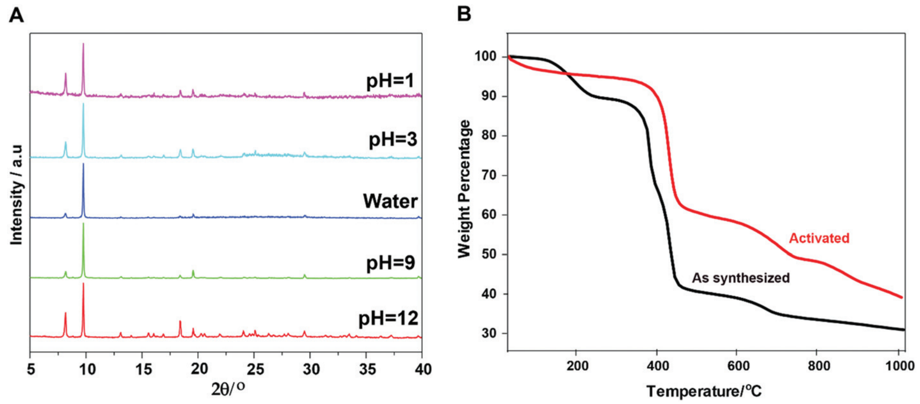

Fig. 3 (A) PXRD patterns of AUBM-1 crystals immersed in aqueous solutions at different pH values and (B) TGA curves of the as-synthesized and activated AUBM-1.

surface area could be attributed to the presence of the charged species within the pores. In addition, the acid and base treatments did not alter much the porous structure of AUBM-1. The BET surface area measurements after the acid and base treatments also confirmed the high chemical stability of the AUBM-1 structure (Fig. S3†).

The IR spectra for free linker, the as-synthesized MOF and the activated one were recorded and are shown in Fig. S3.† Indeed, the COO^- symmetric vibration for 1,2,4,5-benzenetetracarboxylic acid shifts to a lower wavenumber from 1717 to 1629 cm^{-1} for the synthesized MOF. This proves that the carboxylic acid groups are involved in the coordination of the indium metal. Furthermore, the characteristic peaks of 2-methyl imidazole were found in the spectrum of the as-synthesized MOF. The vibrational bands at 1503 and 1507 cm^{-1} characteristic of the C=N were detected as well (Fig. S3†). SEM-EDX analysis of the as-synthesized and activated MOFs revealed that both frameworks contain nitrogen based species from the methyl-imidazolium that is balancing the charge of the framework (Fig. S4 and S5†). This was further confirmed by the TGA-FTIR and NMR experiments. The TGA-FTIR of the AUBM-1 showed the release of ammonia upon burning both the as-synthesized and activated frameworks (Fig. S6†). While, the ^{1}H-NMR of the digested activated MOF compared to that of free methyl-imidazole and pyromellitic acid revealed the existence of both species within the AUBM-1 structure (Fig. S7†).

The high chemical stability of AUBM-1 in aqueous media ($1 \le pH \le 14$) prompted us to study its capability to remove As from water. To this end, arsenate adsorption experiments were performed at different pH values. Arsenate can exist in different oxidation states depending on the pH value. For pH < 2.1, H_3AsO_4 is predominant, and as the pH increases from 2.1 to 6.7, $H_2AsO_4^-$ form is present. Finally, at pH > 6.7, $HAsO_4^{2-}$ form is the predominant species.[11]

In order to find the optimal pH for As removal, the pH was varied between 2 and 10 as shown in Fig. 4. And the best performance of AUBM-1 for As removal was found at neutral pH (7–8) where arsenate exists as $HAsO_4^{2-}$. This high performance at neutral pH makes our MOF material a promising and practical adsorbent for water decontamination. In order to understand the relationship between the surface charges and the MOF adsorption performance, zeta potential analysis was carried out and the obtained values are plotted in Fig. S8.† These results showed that the AUBM-1 surface is negatively charged for a wide range of pH (between 3.0 and 9.0) which demonstrates that the adsorption process was not controlled by simple electrostatic interactions. Interestingly, we noticed that MOF crystals change the neutral pH of water from 6.7 to 4.3 which can be attributed to the strong acidity of the AUBM-1 framework. Therefore, the high As uptake may be explained by the chemical acid–base interactions between the arsenates and the acid sites in the MOF structure.

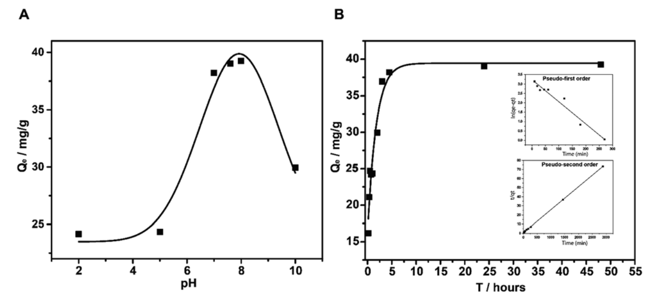

Fig. 4 (A) Adsorption of As at different pH values and (B) adsorption of As at different contact times and the kinetics rate fits; T = 25 °C, $m_{(MOF)}$ = 10 mg; [As] = 40 mg L^{-1}.

Adsorption kinetics

In order to determine the equilibrium adsorption time and study the kinetics of the adsorption process by the MOF structure, the As(v) uptake by the MOF crystals was investigated as a function of contact time. The obtained results are shown in Fig. 4B. For this experiment, 10 mg of MOF crystals were added to a 10 ml aqueous As solution (C_o = 40 mg L^{-1} and pH = 7.6). With time, the concentration of As(v) in the solution decreases until it reaches equilibrium after 3 hours and the adsorption capacity at equilibrium was calculated to be

37 mg g^{-1}. It is evident from Fig. 4B that the adsorption of As is rapid initially and then decreases progressively until equilibrium is reached. Thus, the adsorption was faster at the beginning due to the availability of numerous vacant adsorption sites in the MOF structure.[31]

Pseudo-first-order (eqn (1)) and pseudo-second-order (eqn (2)) models were plotted *via* the two equations respectively, in order to analyze the adsorption kinetics shown in Fig. 4B.

$$\ln(q_\mathrm{e} - q_t) = \ln q_\mathrm{e} - K_1 t \tag{1}$$

$$\frac{t}{q_t} = \frac{1}{K_2 {q_\mathrm{e}}^2} + \frac{t}{q_\mathrm{e}} \tag{2}$$

where q_e (mg g^{-1}) is the equilibrium capacity calculated experimentally, q_t (mg g^{-1}) is the adsorption amount at time t, K_1 (min^{-1}) is the pseudo-first-order rate constant and K_2 (g mg^{-1} min^{-1}) is the pseudo-second-order rate constant. The inset in Fig. 4B depicts the fitting data of the obtained results. The pseudo-second-order model shows higher correlation coefficients (R^2) compared to the pseudo-first-order (0.9999 > 0.9616), and the calculated q_e value from the pseudo-second-order kinetic model (39 mg g^{-1}) is in good agreement with the experimental q_e value (37 mg g^{-1}). Thus, the kinetic adsorption follows the pseudo-second order model. This indicates that the arsenates are strongly adsorbed onto the surface of the frameworks and the chemisorption process is significant.[31]

In order to describe the overall rate of the adsorption process, an intra-particle diffusion model was used. The intra-particle diffusion model correlates with the amount adsorbed at time t (q_t) by (eqn (3)):

$$q_t = k_\mathrm{id} \cdot t^{1/2} + \theta \tag{3}$$

where k_id is the intra-particle diffusion rate constant (mg (g min$^{1/2}$)$^{-1}$), and θ is a constant related to the thickness of the boundary layer (mg g^{-1}).

Fig. S9† shows that the adsorption rates are multistage-controlled processes and are represented by three steps. The first step is attributed to the diffusion of As through the solution to the external surface of the MOF structure. The second step describes the gradual adsorption of As in AUBM-1. The last step is attributed to the diffusion of arsenate molecules on the active sites until equilibrium is attained. From the slope of the intraparticle diffusion, the rate constants of the three linear steps were calculated to be 3.687, 2.201 and 0.0187 mg (g min$^{1/2}$)$^{-1}$, for the first, second and third linear plots respectively. Therefore, the first step is the fastest step, and the intraparticle diffusion is the rate limiting step during the adsorption process.[32]

Adsorption isotherm

The amount of As adsorbed for different initial concentrations onto AUBM-1 was measured and the results are shown in Fig. 5. In this experiment, 10 mg of adsorbent were added to 10 mL aqueous solutions of As concentrations ranging from 30 to 200 mg L^{-1} at T = 25 °C. The adsorption capacity increased as the concentration of As(v) in the solution increased until it

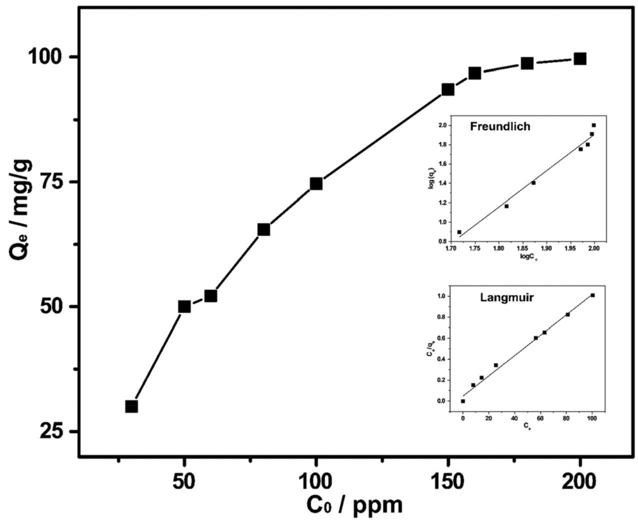

Fig. 5 As uptake by AUBM-1 at different concentrations (25 mg L^{-1} ≤ [As] ≤ 200 mg L^{-1}) from water; $m_{(\mathrm{MOF})}$ = 10 mg; T = 25 °C. Inset: Data fitting using Freundlich and Langmuir models.

reached saturation at 180 mg L^{-1}. This indicates that a higher driving force for mass transfer at higher concentrations of As is responsible for the increase in the As uptake. Since more As ions are available per unit surface area at higher concentrations, the probability of surface adsorption increases. Whereas, after 180 mg L^{-1}, the maximum adsorption capacity reaches 103.1 mg g^{-1}, which corresponds to the adsorption saturation.

Furthermore, the obtained data were evaluated by the following two models, Langmuir (eqn (4)) and Freundlich (eqn (5)) as shown in the inset of Fig. 5.

$$\frac{C_\mathrm{e}}{q_\mathrm{e}} = \frac{C_\mathrm{e}}{q_\mathrm{m}} + \frac{1}{K_\mathrm{L} q_\mathrm{m}} \tag{4}$$

$$\log q_\mathrm{e} = \log K_\mathrm{F} + \frac{1}{n} \log C_\mathrm{e} \tag{5}$$

where q_e (mg g^{-1}) is the amount adsorbed at equilibrium, C_e (mg g^{-1}) is the concentration of adsorbate at equilibrium, q_m is the maximum adsorption capacity, K_L (L mg^{-1}) is an equilibrium constant related to the binding strength, n and K_F (L mg^{-1}) are Freundlich constants that indicate the adsorption capacity and adsorption intensity, respectively.

The inset in Fig. 5 depicts the fitting data of the obtained results. The Langmuir model shows higher correlation coefficients (R^2) (0.9915 > 0.979) which indicates a monolayer adsorption process in this case. Thus, q_m is calculated to be 103.1 mg g^{-1} from the Langmuir equation. By comparing the adsorption capacity of AUBM-1 with that found in the literature, AUBM-1 shows higher uptake than the commercial adsorbents[33,34] and synthetic adsorbents[11–13,35–38] as shown in Table 1.

Thermodynamic analysis

Fig. S10† shows the effect of temperature on the As adsorption from water. As the temperature increases from 25 to 50 °C the adsorption capacity increases which indicates that the arsenate

Table 1 Comparison of arsenate adsorption among prevailing adsorbents

Adsorbent	Max. adsorption capacity mg g^{-1}	Ref.
Commercial TiO_2	14.2	33
Activated alumina grains	15.9 at pH 5	38
MIL-53(Fe)	21.3 at pH 5	13
ZIF-8	60 at pH 7	12
Fe–Mn binary oxide	69.8 at pH 5	36
Nanostructured iron(III)–copper(II) binary oxide	82.7 at pH 7	37
Amorphous zirconium oxide nanoparticles	95 at pH 2	35
UiO-66	303.34 at pH 2 147.71 at pH 7	11
AUBM-1	103.1	This study

removal by AUBM-1 is an endothermic process. The thermodynamic analysis was assessed using the Van't Hoff equation (eqn (6)). The adsorption enthalpy and entropy were calculated by plotting $\ln K$ *vs.* $\frac{1}{T}$ as shown in Fig. 6 and are equal to 25.08 kJ mol^{-1} and 0.052 kJ mol^{-1} K^{-1}, respectively. The positive value for enthalpy change (ΔH_{ads}) confirms that the adsorption process is endothermic. In addition, it suggests a strong interaction between the arsenate anions and the acid sites of the frameworks, which indicates that arsenate anions are mostly chemisorbed onto the surface of the AUBM-1 framework.[31] The Gibbs free energy at different temperatures was calculated and is shown in Table 2.

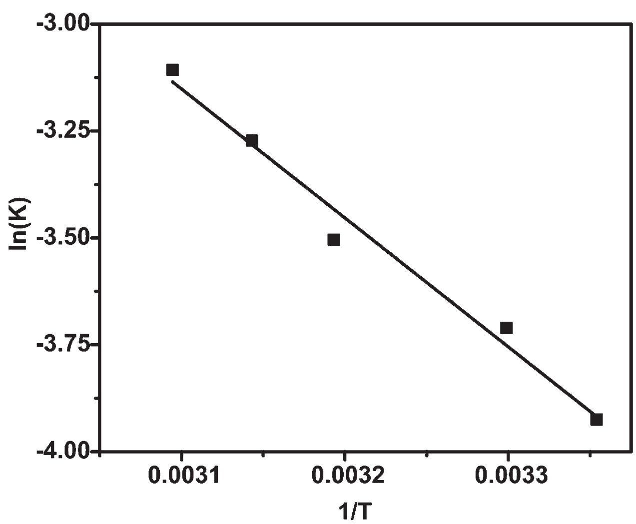

Fig. 6 Van't Hoff plot of ln(*K*) *vs.* 1/*T*.

Table 2 Thermodynamic parameters of As adsorption over activated AUBM-1 at different temperatures

$\Delta H°$ (kJ mol^{-1})	$\Delta S°$ (kJ mol^{-1} K^{-1})	$\Delta G°$ (kJ mol^{-1}) 298 K	303 K	313 K	318 K	323 K
25.08	0.052	+9.74	+9.48	+8.96	+8.71	+8.45

$$\ln K_L = \frac{\Delta S°}{R} - \frac{\Delta H°}{RT} \quad (6)$$

The Gibbs free energy at each temperature was determined as shown in Table 2 using eqn (7):

$$\Delta G° = \Delta H° - T\Delta S° \quad (7)$$

Moreover, the used AUBM-1 sample after the adsorption test under optimal conditions was examined by SEM-EDX, FTIR and TGA. It is evident from Fig. 7 that the framework morphology was preserved and didn't change during the adsorption process. The SEM-EDX of the used adsorbent verifies the presence of As species within the AUBM-1 framework. Adsorption of As was also confirmed by FTIR as shown in Fig. S11.† The adsorbed As(V) spectra showed two bands at 749 and 823 cm^{-1} corresponding to ν(As–O–In) and ν(As–O).[39] In addition, a small peak at 668 cm^{-1} is identified, which would be due to the presence of the As–OH asymmetric stretching.[11,40] Finally, the TGA for the activated sample after As(V) adsorption shows two decomposition steps, which are attributed to the adsorption of As in the pores (Fig. S12†). These data are in good agreement with the thermodynamic and kinetic studies which reveal strong interactions between the arsenate anions and the acidic sites in the AUBM-1 framework.

In order to test the applicability of AUBM-1 as a sorbent for water treatment, the coexistence of other anions should be considered because they may compete with arsenic for the adsorptive sites on the surface of the sorbent. To this end, As removal experiments in the presence of CO_3^{2-} and NO_3^- were performed. The obtained results are shown in Fig. S13.† Two different concentrations of anions were used (1 mM and 10 mM). The results show that the presence of NO_3^- decreases slightly the performance of AUBM-1, which may be due to the similar adsorption behavior between arsenic and nitrates. However, the carbonates enhance its performance. This interesting result can be explained by the increase in the pH of the medium to reach the optimum range (6.5–8.5). Furthermore, the presence of Pb cations in the solution was also tested and the results showed that 55% of the initial As concentration and 45% of Pb were simultaneously removed by AUBM-1. The SEM-EDX analysis of the MOF used in this experiment showed that both elements are adsorbed on the surface of AUBM-1 crystals (Fig. S14†). This indicates that In-MOF is not highly selective for As removal under the employed experimental conditions.

Since the treatment of a low concentration of As in drinking water is a great environmental issue to be solved, we tested our MOF for the removal of ultra-trace As(V) from water. In this experiment, an As concentration of 40 ppb was used and the mass of AUBM-1 was varied between 5 mg and 20 mg (Fig. S15†). Interestingly, 98% of the As were removed by AUBM-1 regardless of the amount of the adsorbent used. This demonstrates the high affinity of the acidic sites in the MOF toward As at low concentrations. However, for the 40 ppm solutions, the adsorption was highly dependent on the mass of the adsorbent and the maximum As removal (80%) was achieved

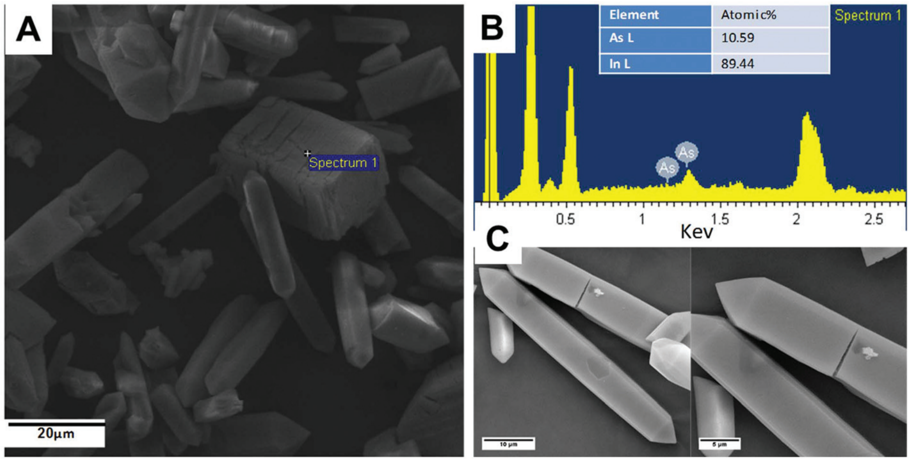

Fig. 7 SEM-EDX of AUBM-1 after adsorption studies reveal the presence of As on the surface of the crystals (A and B). HRSEM images of AUBM-1 crystals after the adsorption studies demonstrate that the morphology of the MOF is preserved (C).

by using 20 mg of MOF. Indeed, for high As concentrations, the available adsorption sites are limited, therefore more adsorbent is needed to remove the high As concentration.

Desorption of As from the MOF adsorbent was performed by using a concentrated NaCl solution and approximately 80% of the As was successfully desorbed after each cycle (Fig. 8), and without affecting the integrity of the framework as evidenced by the PXRD pattern of the recovered MOF crystals (Fig. S16†). Interestingly, the recovered MOF crystals were successfully used to remove As from water with a slight decrease (25%) in the performance after the third cycle due to the decrease in the available adsorption sites after 3 cycles. Thus our In-MOF can be used as a potential recyclable adsorbent for As removal.

In conclusion, a new chemically stable In-MOF (AUBM-1) of **pts** topology was synthesized and thoroughly characterized. Due to its chemical stability, it was applied as an adsorbent for the removal of As from water at neutral pH. The process achieved an impressive arsenate uptake capacity of 103.1 mg g^{-1} which is higher than the commercial adsorbents and some synthetic adsorbents. The kinetics of As adsorption followed a pseudo-second-order kinetic model and the thermodynamic study revealed that the adsorption of As was an endothermic process with a ΔH value of 25.08 kJ mol^{-1}.

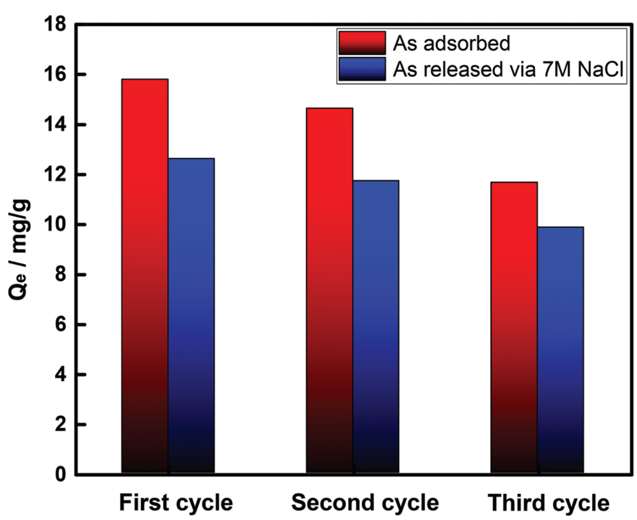

Fig. 8 Removal of As from water after regeneration of AUBM-1 for three cycles. $[As]_0$ = 25 mg L^{-1}; m_{AUBM-1} = 10 mg.

Conflicts of interest

There are no conflicts to declare.

Acknowledgements

We gratefully acknowledge the funding provided by the American University of Beirut Research Board, the Masri Institute (# 103214) and the K. Shair Central Research Science Laboratory. We thank Ms Boushra Mortada and Zeinab Kara Ali for their assistance in the experimental work and Dr Felipe Gandara for the valuable discussion.

References

1 H.-C. Zhou, J. R. Long and O. M. Yaghi, *Chem. Rev.*, 2012, **112**, 673–674.
2 C. A. Trickett, A. Helal, B. Al-maythalony, Z. H. Yamani, K. Cordova and O. M. Yaghi, *The chemistry of metal–organic frameworks for CO_2 capture, regeneration and conversion*, 2017.
3 M. Hmadeh, Z. Lu, Z. Liu, F. Gándara, H. Furukawa, S. Wan, V. Augustyn, R. Chang, L. Liao, F. Zhou, E. Perre, V. Ozolins, K. Suenaga, X. Duan, B. Dunn, Y. Yamamto, O. Terasaki and O. M. Yaghi, *Chem. Mater.*, 2012, **24**, 3511–3513.

4 K. Adil, Y. Belmabkhout, R. S. Pillai, A. Cadiau, P. M. Bhatt, A. H. Assen, G. Maurin and M. Eddaoudi, *Chem. Soc. Rev.*, 2017, **46**, 3402–3430.

5 Z. Moussa, M. Hmadeh, M. Abiad, O. H. Dib and D. Patra, *Encapsulation of curcumin in cyclodextrin-metal organic frameworks: Dissociation of loaded CD-MOFs enhances stability of curcumin*, 2016.

6 B. Mortada, T. A. Matar, A. Sakaya, H. Atallah, Z. Kara Ali, P. Karam and M. Hmadeh, *Inorg. Chem.*, 2017, **56**, 4739–4744.

7 M. Al-Ghoul, R. Issa and M. Hmadeh, *CrystEngComm*, 2017, **19**, 608–612.

8 P. Horcajada, R. Gref, T. Baati, P. K. Allan, G. Maurin, P. Couvreur, G. Férey, R. E. Morris and C. Serre, *Chem. Rev.*, 2012, **112**, 1232–1268.

9 J. A. Mason, M. Veenstra and J. R. Long, *Chem. Sci.*, 2014, **5**, 32–51.

10 S. Furukawa, J. Reboul, S. Diring, K. Sumida and S. Kitagawa, *Chem. Soc. Rev.*, 2014, **43**, 5700–5734.

11 C. Wang, X. Liu, J. P. Chen and K. Li, *Sci. Rep.*, 2015, **5**, 16613.

12 M. Jian, B. Liu, G. Zhang, R. Liu and X. Zhang, *Colloids Surf., A*, 2015, **465**, 67–76.

13 T. A. Vu, G. H. Le, C. D. Dao, L. Q. Dang, K. T. Nguyen, Q. K. Nguyen, P. T. Dang, H. T. K. Tran, Q. T. Duong, T. V. Nguyen and G. D. Lee, *RSC Adv.*, 2015, **5**, 5261–5268.

14 K. Jomova, Z. Jenisova, M. Feszterova, S. Baros, J. Liska, D. Hudecova, C. J. Rhodes and M. Valko, *J. Appl. Toxicol.*, 2011, **31**, 95–107.

15 J. W. Jun, M. Tong, B. K. Jung, Z. Hasan, C. Zhong and S. H. Jhung, *Chemistry*, 2015, **21**, 347–354.

16 M. Jian, H. Wang, R. Liu, J. Qu, H. Wang and X. Zhang, *Environ. Sci.: Nano*, 2016, **3**, 1186–1194.

17 A. H. Smith and C. M. Steinmaus, *Annu. Rev. Public Health*, 2009, **30**, 107–122.

18 N. Nicomel, K. Leus, K. Folens, P. Van Der Voort and G. Du Laing, *Int. J. Environ. Res. Public Health*, 2016, **13**(1), 62.

19 D. Mohan and C. U. Pittman Jr., *J. Hazard. Mater.*, 2007, **142**, 1–53.

20 P. Pusztai, E. Tóth-Szeles, D. Horváth, Á. Tóth, Á. Kukovecz and Z. Kónya, *CrystEngComm*, 2015, **17**, 8477–8485.

21 G. Zhang, X. Li, S. Wu and P. Gu, *Environ. Earth Sci.*, 2012, **66**, 1269–1277.

22 Y. Liu, J. F. Eubank, A. J. Cairns, J. Eckert, V. Kravtsov, R. Luebke and M. Eddaoudi, *Angew. Chem., Int. Ed.*, 2007, **46**, 3278–3283.

23 Z. B. Han, B. Y. Li, J. W. Ji, Y. E. Du, H. Y. An and M. H. Zeng, *Dalton Trans.*, 2011, **40**, 9154–9158.

24 L. M. Aguirre-Díaz, D. Reinares-Fisac, M. Iglesias, E. Gutiérrez-Puebla, F. Gándara, N. Snejko and M. Á. Monge, *Coord. Chem. Rev.*, 2017, **335**, 1–27.

25 O. Delgado-Friedrichs, M. O'Keeffe and O. M. Yaghi, *Acta Crystallogr., Sect. A: Found. Crystallogr.*, 2006, **62**, 350–355.

26 L. Zhu, D. Zhang, M. Xue, H. Li and S. Qiu, *CrystEngComm*, 2013, **15**, 9356.

27 H. Deng, S. Grunder, K. E. Cordova, C. Valente, H. Furukawa, M. Hmadeh, F. Gándara, A. C. Whalley, Z. Liu, S. Asahina, H. Kazumori, M. O'Keeffe, O. Terasaki, J. F. Stoddart and O. M. Yaghi, *Science*, 2012, **336**(6084), 1018–1023.

28 D. Feng, W. C. Chung, Z. Wei, Z. Y. Gu, H. L. Jiang, Y. P. Chen, D. J. Darensbourg and H. C. Zhou, *J. Am. Chem. Soc.*, 2013, **135**, 17105–17110.

29 K. S. Park, Z. Ni, A. P. Cote, J. Y. Choi, R. Huang, F. J. Uribe-Romo, H. K. Chae, M. O'Keeffe and O. M. Yaghi, *Proc. Natl. Acad. Sci. U. S. A.*, 2006, **103**, 10186–10191.

30 S. Huh, T. H. Kwon, N. Park, S. J. Kim and Y. Kim, *Chem. Commun.*, 2009, 4953–4955, DOI: 10.1039/b905138d.

31 E. García, R. Medina, M. Lozano, I. Hernández Pérez, M. Valero and A. Franco, *Materials*, 2014, **7**, 8037–8057.

32 A. Goswami, P. K. Raul and M. K. Purkait, *Chem. Eng. Res. Des.*, 2012, **90**, 1387–1396.

33 J.-S. Hu, L.-S. Zhong, W.-G. Song and L.-J. Wan, *Adv. Mater.*, 2008, **20**, 2977–2982.

34 Y. Hamzeh, A. Ashori, E. Azadeh and A. Abdulkhani, *Mater. Sci. Eng., C*, 2012, **32**, 1394–1400.

35 H. Cui, Q. Li, S. Gao and J. K. Shang, *J. Ind. Eng. Chem.*, 2012, **18**, 1418–1427.

36 G. Zhang, J. Qu, H. Liu, R. Liu and R. Wu, *Water Res.*, 2007, **41**, 1921–1928.

37 G. Zhang, Z. Ren, X. Zhang and J. Chen, *Water Res.*, 2013, **47**, 4022–4031.

38 T. Lin and J. Wu, *Water Res.*, 2001, **35**, 2049–2057.

39 W. Zhu, X. Cui, X. Liu, L. Zhang, J. Q. Huang, X. Piao and Q. Zhang, *Nanoscale Res. Lett.*, 2013, **8**, 2.

40 N. Mahanta and J. P. Chen, *J. Mater. Chem. A*, 2013, **1**, 8636.